Hindawi
Complexity
Volume 2019, Article ID 7465461, 11 pages
https://doi.org/10.1155/2019/7465461

Research Article

Jiles-Atherton Based Hysteresis Identification of Shape Memory Alloy-Actuating Compliant Mechanism via Modified Particle Swarm Optimization Algorithm

Le Chen[1,2] **Ying Feng**[1,2] **Rui Li**[1,2] **Xinkai Chen**[3] **and Hui Jiang**[4]

[1]*College of Automation Science and Engineering, South China University of Technology, Guangzhou, Guangdong 510641, China*
[2]*Key Laboratory of Autonomous Systems and Networked Control, Ministry of Education, South China University of Technology, Guangzhou 510640, China*
[3]*Department of Electronic and Information Systems, Shibaura Institute of Technology, Saitama 337-8570, Japan*
[4]*School of Electronic Engineering and Automation, Guilin University of Electronic Technology, Guilin, Guangxi 541004, China*

Correspondence should be addressed to Ying Feng; zhdfengying@gmail.com

Received 16 August 2018; Revised 31 October 2018; Accepted 18 January 2019; Published 11 February 2019

Guest Editor: Andy Annamalai

Shape memory alloy- (SMA-) based actuators are widely applied in the compliant actuating systems. However, the measured data of the SMA-based compliant actuating system reveal the input-output hysteresis behavior, and the actuating precision of the compliant actuating system could be degraded by such hysteresis nonlinearities. To characterize such nonlinearities in the SMA-based compliant actuator precisely, a Jiles-Atherton model is adopted in this paper, and a modified particle swarm optimization (MPSO) algorithm is proposed to identify the parameters in the Jiles-Atherton model, which is a combination of several differential nonlinear equations. Compared with the basic PSO identification algorithm, the designed MPSO algorithm can reduce the local optimum problem so that the Jiles-Atherton model with the identified parameters can show good agreements with the measured experimental data. The good capture ability of the proposed identification algorithm is also examined through the comparisons with Jiles-Atherton model using the basic PSO identification algorithm.

1. Introduction

Shape memory alloys (SMA) are a class of smart-materials which can be utilized as "artificial muscle" actuating device, imitating the performance of natural muscles [1–3]. Compared with the conventional actuator devices, such as hydraulics and DC motor, the special feature of SMA materials can work around the limitation of low power density and large size in these conventional actuators [4, 5]. Currently, there are several artificial muscle actuators, such as pneumatic artificial muscles [6], electroactive polymers (EAP), and SMA actuators [7, 8]. For the pneumatic systems, they require several peripheral types of equipment such as air compressors, valves, and pressure sensors, and these components make the system bulky and noisy. As for SMA-based actuators, they can provide silent operating condition and do not need the separate pump to provide the energy, which can save the actuating device size and provide better operation environment [8, 9]. Different from EAP actuators, SMA-based actuators with the low-voltage driving mode can be used easily as "muscle" devices. Besides, the flexible shape, wide operation range, and high power to weight ratio are also the good features of the SMA-based compliant actuators and have been applied in microactuating systems, miniature robots, compliant mechanism, and biomedical instruments [10, 11].

The working principle of SMA-based actuators is the energy transformation from thermal energy to mechanical energy with the change of the temperature or vice versa [1]. The heating or cooling of SMA-based actuators will cause the shape deformation of the SMA materials, which creates the smooth stress or strain as the actuating force to the actuated plants, and this output performance can be used as compliant actuators well [12]. In this paper, a different

SMA-based actuator structure introduced in [5] is adopted as the testified platform, and the connecting way of the SMA wires can decrease the stiffness and increase the compliance, showing the muscle-like actuating performance [13].

However, one of the shortcomings of SMA-based compliant actuators is the hysteretic nonlinearity in the process of SMA phase transformation [4]. The thermodynamical characteristics of SMA materials are not reversible, which lead to strong saturated hysteretic behavior. Besides, the delay between the input driving signal and the measured temperature can couple with the internal hysteresis in the SMA materials, causing complex coupling hysteresis nonlinear characteristics in the output of SMA-based compliant actuators [14]. The strong hysteresis nonlinearities decrease the feasibility to implement the SMA-based compliant actuators as muscle-like operation devices. Therefore, the modeling of hysteresis becomes the primary work to improve the actuating precision of SMA-based compliant actuators [14, 15].

Generally, there are two types of hysteresis modeling methods. One is to establish the model based on the physical equations or parameters of the mechanism, such as Stoner-Wohlfarth model and Globus model [16]; another is to build the model based on the input-output relationship of the mechanism, which does not need the physical parameters of the system and can be extended to the different systems easily, for example, Preisach model [17], Prandtl-Ishlinskii model [18, 19], Bouc-Wen model [20], and Jiles-Atherton (J-A) model [21]. Therein, the Jiles-Atherton modeling method originates from the hysteresis description in the magnetic field, and it can provide an accurate description for the strong saturated hysteresis in the SMA-based compliant actuators [22]. Moreover, the Jiles-Atherton model needs less storage compared with other hysteresis modeling methods [23], which is easier for the real-time application. In this paper, the Jiles-Atherton model is adopted to describe the saturated hysteresis in the SMA-based compliant actuators to show the output characteristics of the compliant actuators.

As introduced in [21], the structure of the Jiles-Atherton model is combined with several differential equations, and the output of Jiles-Atherton model is to obtain the analytical solution of these differential equations, so the parameters in the Jiles-Atherton model are not easy to be identified directly by using the common identification method which limits the implementation of the Jiles-Atherton model. Therefore, the parameter identification method of the Jiles-Atherton model is addressed as the primary goal of this study to show the output performance of SMA-based compliant actuators.

To solve the difficulties of the parameter identification in the SMA-based compliant actuators, a modified particle swarm optimization (PSO) algorithm is proposed in this paper. The PSO algorithm is a new computation technique proposed in 1995 [24], which is a class of swarm-based algorithms, starting with a population of random solutions and continuing by improving population using a cost function. Different from the conventional identification algorithms, PSO algorithm can obtain the optimal solution of the parameters in a multidimensional space [25, 26], and it should obtain better solutions of the parameters in the Jiles-Atherton model effectively. Compared with the basic PSO algorithm, the proposed PSO algorithm is designed to reduce the chance of getting trapped in a local optimum. By using the random mutation step for the updating of the parameters in the location and velocity, the parameters of the Jiles-Atherton hysteresis model identified using the modified PSO algorithm can describe the hysteresis nonlinearities in the SMA-based compliant actuators more accurately. To verify the accuracy of the proposed identification method, the experiment is conducted by choosing the PWM signal's cycles as 60s with amplitude 5V and duty cycle as 50%. The experimental comparison results with the basic PSO algorithm with random mutation step illustrate that the proposed identification algorithm behaves better for the SMA-based compliant actuators.

The main content of the paper is as follows: Section 2 introduced the SMA-based compliant actuators discussed in this paper. The Jiles-Atherton hysteresis model adopted to describe the hysteretic nonlinearities in the SMA compliant actuating mechanism is introduced in Section 3. In Section 4, the structures of the basic PSO algorithm and the proposed modified PSO algorithm are presented. The experimental output and the model accuracy evaluation test are given in Section 5 to verify the effectiveness of the proposed identification method. Finally, the conclusion about the proposed identification method for the Jiles-Atherton model is presented in Section 6.

2. SMA-Based Compliant Actuating Platform

In this section, the compliant actuating platform based on SMA actuators is introduced. By changing the temperature, the phase transformation of shape memory alloys from the low-temperature state (martensite phase) into the high-temperature state (austenite phase) or vice versa will stimulate the mechanical force (strain or stress) with the high strength and large recovery strain properties during the activation process (heating process) or the deactivation process (cooling process).

Usually, there are three typical structures: one-way SMA actuator, bias-spring SMA actuators, and different (antagonistic) actuators. One-way SMA actuator and bias-spring SMA actuators have slow response since the deactivation process is determined by the cooling process or the passive spring which leads to the uncontrollable deformation speed. To solve this problem, a different SMA wires structure [5] is used in this study, which consists of two complementary SMA wires, two couplers and a torsion spring. As shown in Figure 1, the antagonist wires can produce the active force to imitate the rotational motion of the human joint in bidirection, and the motion speed can be adjusted by the active contraction force between the SMA wires and the couplers connected by the spring. The advantage of this structure is to get the muscle-like actuating output with functions of high flexibility, lightweight, and noiselessness in the human motor systems.

To show the actuating output of the SMA-based compliant actuating system, the input-output relationship was testified in the experiment device, where the change of temperature acting on the SMA wires could be obtained

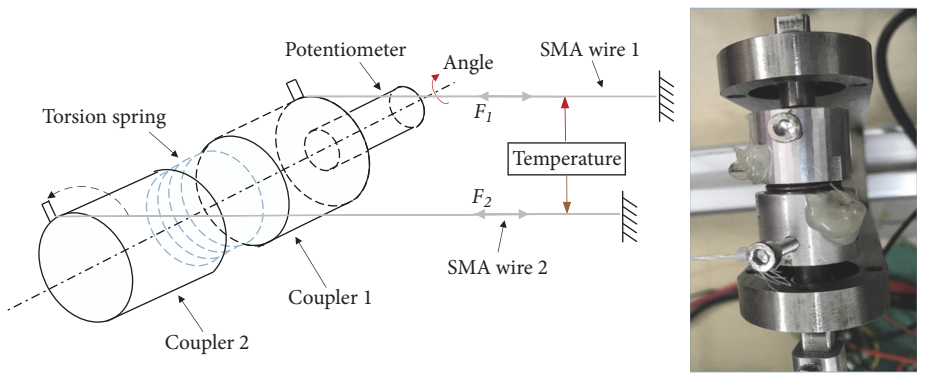

Figure 1: Schematic of the SMA compliant actuating system.

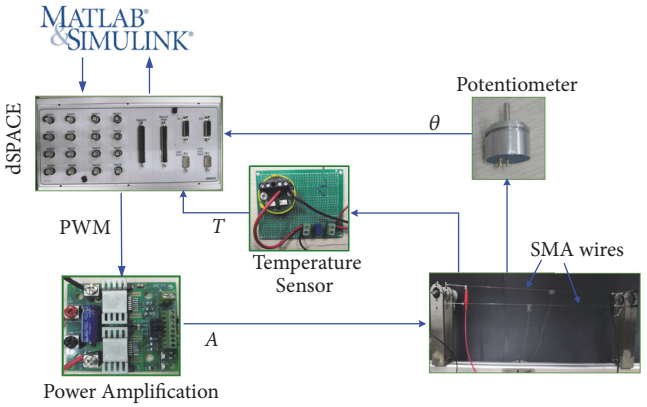

Figure 2: Experimental platform of the SMA-based compliant actuators.

by the driven voltage. As shown in Figure 2, two SMA wires (NiTi SMA wires, 0.25mm) were connected with two cylindrical couplers and a torsion spring to produce the angular motion of the coupler. The actuator displacement was measured by the potentiometer, and the input signal and the temperature applied to the SMA wires and the rotation angle output were acquired in the Control platform (dSPACE 1103).

The open-loop test at the PWM signal cycle was performed to show the input-output characteristics of the SMA-based compliant actuator used in this paper. A fixed duty cycle (50%) PWM signal under amplitude (5V) operation with 50s signal cycle was adopted to produce the temperature changing between 0°C and 60°C, and the angular position of the coupler was measured by a high precision potentiometer. The desired signal (Figure 3(a)), input temperature (Figure 3(b)), and the rotation angle output (Figure 3(c)) are given to show the output characteristics of the SMA-based compliant actuator. According to the input (temperature)-output (rotation angle) relationship, it is obvious that strong saturation-type hysteresis nonlinearities caused by the phase transformation exist in the SMA materials, and the result is given in Figure 3(d).

Remark 1. According to the experiment results of the open-loop test, the hysteresis in the SMA-based compliant actuator with strong saturation property and some hysteresis modeling methods cannot cover this special characteristic, for example, conventional Prandtl-Ishlinskii model [19] and Backlash-like model [27]. The existence of the saturated hysteresis will degrade the output performance of the SMA-based compliant actuator, and the modeling of hysteresis becomes a primary step to improve the actuating performance. In this paper, a Jiles-Atherton model is employed as an illustration to show the way of dealing with the strong hysteresis nonlinearities.

3. Hysteresis Modeling with Jiles-Atherton Model

The Jiles-Atherton model [21, 23] is a typical hysteresis model, which is derived from ferromagnetic magnetization theory to show the relationship between applied magnetic field H and magnetization M by considering the nonmagnetic impurity, grain boundary, residual stress, and the hysteresis. In this section, the Jiles-Atherton model is introduced briefly. It enables the mathematical description of hysteresis curves between magnetic flux intensity B and magnetic field intensity H with five parameters [28].

Usually, magnetization M includes two components, reversible magnetization M_{rev} and irreversible magnetization M_{irr}:

$$M_{rev} = c\left(M_{an} - M_{irr}\right) \tag{1}$$

where M_{rev} and M_{irr} can be obtained by the anhysteretic magnetization M_{an} which is produced by the rotation of the magnetic domain. c is the magnetization weighting factor. The anhysteretic magnetization can be provided by the Langevin function:

$$M_{an} = M_s\left[\coth\left(\frac{H_{eff}}{a}\right) - \frac{a}{H_{eff}}\right] \tag{2}$$

where M_s is the saturation magnetization, a is the anhysteretic form factor, and H_{eff} is the Weiss effective field defined as

$$H_{eff} = H + \alpha M \tag{3}$$

$$M_{irr} = \frac{M - cM_{rev}}{1 - c} \tag{4}$$

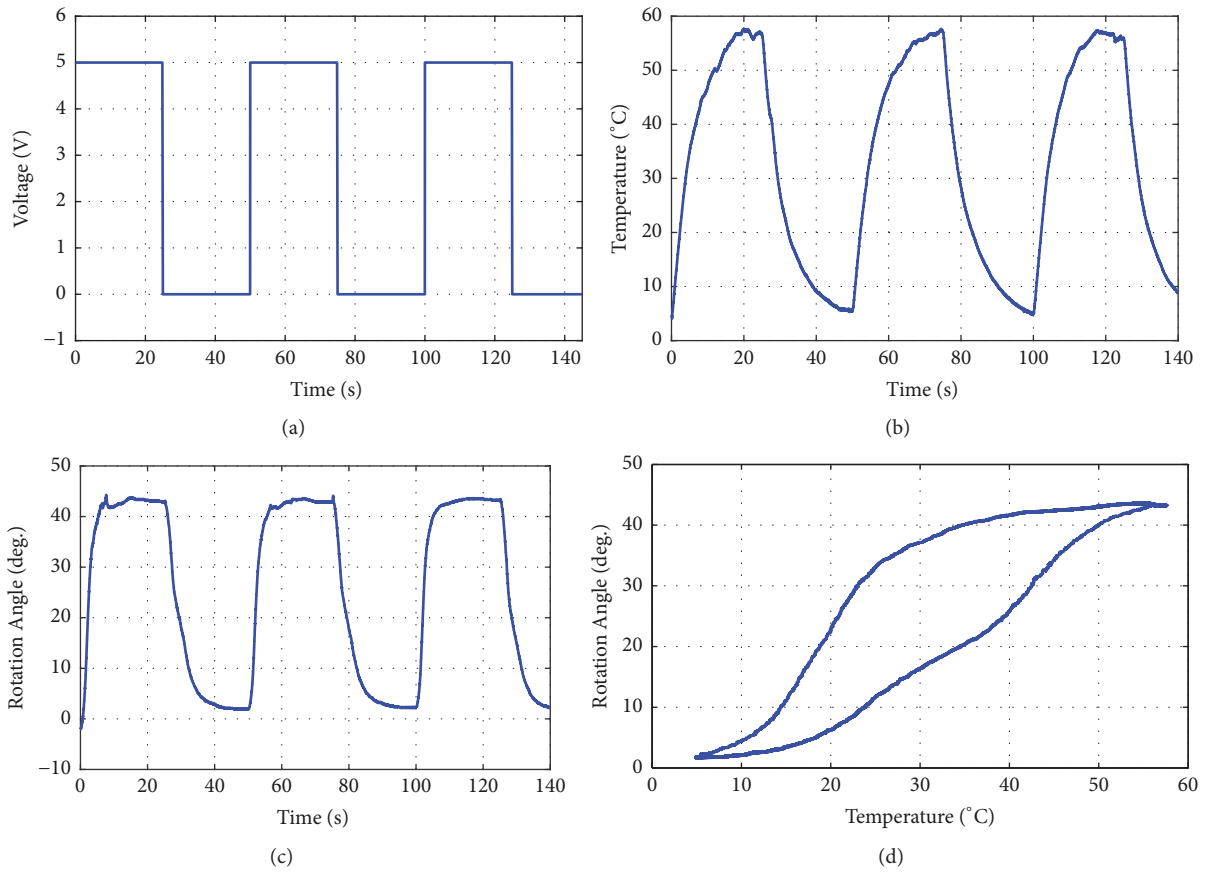

FIGURE 3: Input-output characteristics of the SMA-based compliant actuators under a fixed duty cycle (50%) 5v PWM signal operation with 50s signal cycle producing the temperature changing between 0°C and 60°C. (a) Input desired signal (voltage). (b) Input temperature. (c) Output rotation angle. (d) Hysteresis loop.

Regarding the energy dissipation, the differential expression of the irreversible magnetization M_{irr} is given as

$$\frac{dM_{irr}}{dH} = \frac{M_{an} - M_{irr}}{k\delta - \alpha\left(M_{an} - M_{irr}\right)} \tag{5}$$

where δ is a direction parameter to show the ascending and descending of the hysteresis loop as

$$\delta = \operatorname{sgn}\left(\frac{dH}{dt}\right) = \begin{cases} 1 & \dfrac{dH}{dt} > 0 \\ -1 & \dfrac{dH}{dt} < 0 \end{cases} \tag{6}$$

The anhysteretic magnetization M_{an} is calculated by considering the thermodynamics of the magnetostrictive material. The reversible magnetization M_{rev} calculates the extent of bulging of domain walls before they acquire the energy required to escape the inclusions. It is defined as

$$M_{rev} = c\left(M_{an} - M_{irr}\right) \tag{7}$$

Then it can be deduced since the amount of bending of the domain

$$\frac{dM_{rev}}{dH} = c\left(\frac{dM_{an}}{dH} - \frac{dM_{irr}}{dH}\right) \tag{8}$$

Summation of the reversible and irreversible components of the differential components leads to the total differential susceptibility of dM/dH:

$$\frac{dM}{dH} = (1-c)\frac{M_{an} - M_{irr}}{k\delta - \alpha\left(M_{an} - M_{irr}\right)} + c\frac{dM_{an}}{dH} \tag{9}$$

$$M = M_{rev} + M_{irr} \tag{10}$$

$$M = cM_{an} + (1-c)M_{irr} \tag{11}$$

$$M_{irr} = \frac{1}{1-c}\left(M - cM_{an}\right) \tag{12}$$

where α, a, c, k, and M_s are the parameters of Jiles-Atherton hysteresis model. c is the coefficient of reversibility of the movement of the walls, a is the form factor, M_s is the saturation magnetization, and α and k represent the interaction between the domains and the hysteresis losses, respectively. The hysteresis output which is defined in the magnetic field is the magnetic flux intensity B, and it can be obtained using the relationship between B and M as $B = \mu_0(H + M)$ with μ_0

as $\pi \cdot 4 \cdot 10^{-7}$. Finally, the hysteresis curve is represented by the mathematical expression of $H - B$.

Remark 2. Compared with other hysteresis models, Jiles-Atherton model can formulate the hysteresis by several differential equations related to the behavior of ferromagnetic materials, so it is easy to describe the hysteresis of the SMA-based compliant actuators with strong saturation. Besides, the structure of the Jiles-Atherton model is based on the differential equations requiring less memory storage, which makes it convenient for the real-time application.

As introduced, the parameter identification is significant to make good use of Jiles-Atherton model describing hysteresis in SMA materials. For such purpose, the identification process is discussed in Section 4 in detail.

4. Parameter Identification Based Modified PSO Algorithm

The classic method for the parameter identification of Jiles-Atherton model had been discussed in some literature [22, 26]. Considering the differential-equation based structure of Jiles-Atherton model, the iterative identification algorithm causes the problems of being sensitive to the initial values of the model parameters, and the common identification algorithm may not converge or get trapped in local optimum in some special cases [25]. To solve the existing identification problems in Jiles-Atherton model, an artificial intelligence method is implemented in this paper. In this section, a modified particle swarm optimization (MPSO) is proposed.

4.1. Basic PSO Algorithm. For particle swarm optimization algorithm [25, 26, 29], each particle is associated with a position, a velocity, and a fitness value which depends on the optimization function. The particle updates itself by following two extreme values in every iteration. One is the optimal solution found by the particle itself, called personal extreme point (Pbest). The other one is called global extreme point (Gbest) which is the overall optimal solution. The basic PSO method is introduced briefly in this section.

In the basic PSO algorithm, every candidate solution is treated as a particle point in a D-dimensional space [24]. Accordingly, the position of i-th particle can be represented by a D-dimensional vector

$$\mathbf{x}_i = \begin{bmatrix} x_{i1} & x_{i2} & x_{i3} & \cdots & x_{iD} \end{bmatrix} \tag{13}$$

and the population of N candidate solutions constructs the vector $\mathbf{X}$ which is treated as a swarm

$$\mathbf{X} = \{\mathbf{x}_1, \ \mathbf{x}_2, \ \ldots, \ \mathbf{x}_N\} \tag{14}$$

To obtain the optimal solution, the trajectories of particles in the search space can follow the motion equation as

$$\mathbf{x}_i (n+1) = \mathbf{x}_i (n) + \mathbf{v}_i (n+1) \tag{15}$$

where n and $n+1$ are the algorithm iterations, and the velocities of the particle $\mathbf{v}_i$ along the D-dimensions are defined as

$$\mathbf{v}_i = \begin{bmatrix} v_{i1} & v_{i2} & v_{i3} & \cdots & v_{iD} \end{bmatrix} \tag{16}$$

which can be treated as bounded in the rage $\mathbf{v}_{ij} \in [-v_{\max}, v_{\max}]$, $v_{\max}$ is the given maximum velocity, and $j = 1, 2, \ldots, D$.

The velocity vectors determine the moving direction of the particles which is described as

$$\begin{aligned} \mathbf{v}_i (n+1) = {} & \Lambda \mathbf{v}_i (n) + c_1 \mathbf{R}_1 \left(\mathbf{p}_i - \mathbf{x}_i (n)\right) \\ & + c_2 \mathbf{R}_2 \left(\mathbf{p}_g - \mathbf{x}_i (n)\right) \end{aligned} \tag{17}$$

where $\mathbf{p}_i$ is the personal extreme point (Pbest) previously visited of the i-th particle which is defined as

$$\mathbf{p}_i = \left[p_{i1}, p_{i2}, \ldots, p_{iD}\right], \quad i = 1, 2, \ldots, N \tag{18}$$

and $\mathbf{p}_g$ defined in (19) is the global extreme point (Gbest) of the particle swarm

$$\mathbf{p}_g = \left[p_{g1}, p_{g2}, \ldots, p_{gD}\right] \tag{19}$$

N is the size of the swarm, and Λ is the inertia weight, which is generally between 0.8 and 1.2. c_1 and c_2 are the cognitive and the social parameters, which are nonnegative constants and are chosen in the range $0 \le c_1, c_2 \le 4$. Usually, $c_1 = c_2 = 2$ can satisfy most of the applications [24]. $\mathbf{R}_1$ and $\mathbf{R}_2$ are diagonal matrices of random numbers being generated in $[0, 1]$.

The purpose of the identification is to minimize the error between the measured system output $\mathbf{y}_o(n)$ and the calculated output $\mathbf{y}(n)$. A fitness function of the particle i is defined as

$$\text{Fitness} = J = \frac{1}{\mathrm{E}} \sqrt{\sum_{i=1}^{\mathrm{E}} \left(\frac{y_i - y_{0i}}{y_{o\max}}\right)^T \left(\frac{y_i - y_{0i}}{y_{o\max}}\right)} \tag{20}$$

where E is the number of measurement points used for the parameter identification. $y_{o\max}$ is the maximum of the measured M sets of system output data.

4.2. Modified PSO Algorithm. In practical applications, the basic PSO algorithm shows some problems, such as premature convergence and poor local search ability. It is necessary to do some improvements for this identification method. In this paper, a modified PSO algorithm is proposed to reduce the local optimum problem in the basic PSO algorithm. The details are given as follows.

In the modified PSO algorithm, an iteration-varying inertia weight $\Lambda(n)$ is adopted for the velocity term of update

equations, and the velocity and position of the i-th particle are defined as

$$\mathbf{v}_i(n+1) = \Lambda(n)\,\mathbf{v}_i(n) + c_1\mathbf{R}_1\left(\mathbf{p}_i - \mathbf{x}_i(n)\right) + c_2\mathbf{R}_2\left(\mathbf{p}_g - \mathbf{x}_i(n)\right) \tag{21}$$

$$\mathbf{x}_i(n+1) = \mathbf{x}_i(n) + \mathbf{v}_i(n+1) \tag{22}$$

where n and $n+1$ are the algorithm iterations and $i = 1, 2, ..., N$. The value of the inertia weight $\Lambda(n)$ in (21) is updated using the rule defined in (23) to improve the accuracy.

$$\Lambda(n) = \Lambda_{\max} - \left(\Lambda_{\max} - \Lambda_{\min}\right)\frac{n}{\Xi} \tag{23}$$

where Ξ denotes the maximum iteration number, and $\Lambda_{\min}$ and $\Lambda_{\max}$ represent the selected minimum and maximum values for the inertia weight, respectively, and satisfy $\Lambda_{\max}, \Lambda_{\min} \in (0, 1]$ and $\Lambda_{\max} > \Lambda_{\min}$.

Considering the structure of the Jiles-Atherton model, which is combined by several differential equations, the analytical expression of Jiles-Atherton model cannot be obtained directly. To match the nonlinear feature of the identified model during the calculation process, a novel parameter-varying adjustment strategy is designed in this paper. The cognitive parameter c_1 and the social parameter c_2 both nonlinearly will be changed with the change of the number of iterations:

$$c_1 = c_{1\text{ini}} - \left(c_{1\text{ini}} - c_{1\text{end}}\right)\cdot e^{-70\times((\Lambda-\Lambda_{\min})/(\Lambda_{\max}-\Lambda_{\min}))^6} \tag{24}$$

$$c_2 = c_{2\text{ini}} - \left(c_{2\text{ini}} - c_{2\text{end}}\right)\cdot e^{-70\times((\Lambda-\Lambda_{\min})/(\Lambda_{\max}-\Lambda_{\min}))^6} \tag{25}$$

where $c_{1\text{ini}}$, $c_{2\text{ini}}$ are positive constants for cognitive parameters c_1 and $c_{1\text{end}}$, $c_{2\text{end}}$ are positive parameters for the social parameter c_2 in the modified iteration-varying adjustment strategies in (24) and (25), satisfying $c_{1\text{ini}}, c_{1\text{end}}, c_{2\text{ini}}, c_{2\text{end}} \in (0, 4]$ and $c_{1\text{ini}} \geq c_{2\text{end}} > c_{2\text{ini}} \geq c_{1\text{end}}$, which is related to the inertia weight Λ and design parameters $\Lambda_{\min}$ and $\Lambda_{\max}$.

4.3. MPSO Identification Procedure. In this subsection, the parameter identification process for the Jiles-Atherton hysteresis model based on the modified PSO algorithm is introduced. The optimization process includes 6 steps and the flowchart of the modified PSO algorithm is given in Figure 4.

Step 1. The initiation of each particle is defined for the identified parameters randomly.

$$x_{ij}^{\text{ini}} = x_{\min j} + \left(x_{\max j} - x_{\min j}\right)\times \text{rand}_1 \quad (i = 1, 2, \ldots, N;\ j = 1, 2, \ldots, D) \tag{26}$$

$$v_{ij}^{\text{ini}} = v_{\min j} + \left(v_{\max j} - v_{\min j}\right)\times \text{rand}_2 \quad (i = 1, 2, \ldots, N;\ j = 1, 2, \ldots, D) \tag{27}$$

where x_{ij}^{ini} and v_{ij}^{ini} are the initial values of x_{ij} and v_{ij}, $x_{\max j}$ and $x_{\min j}$ are the maximum and minimum values of the j-th parameter, and $v_{\max j}$ and $v_{\min j}$ are the maximum and minimum values of the j-th parameter update speed. rand_1 and rand_2 are two random numbers with a range of $[0, 1]$.

Step 2. Calculate the fitness function of each particle defined in (20), where B_i is the calculated output and B_{oi} is the measured system output.

$$\text{Fitness} = J = \frac{1}{\text{E}}\sqrt{\sum_{i=1}^{\text{E}}\left(\frac{B_i - B_{0i}}{B_{o\max}}\right)^T\left(\frac{B_i - B_{0i}}{B_{o\max}}\right)} \tag{28}$$

Initialize the values of personal best $\mathbf{p}_i$ of each particle and global best $\mathbf{p}_g$. If $\text{Fitness}(\mathbf{p}_g) > 10^{-7}$, go to Step 6.

Step 3.

For each particle i do

update Λ, c_1 and c_2 using the equations in (23), (24) and (25)

update velocity $\mathbf{v}_i$ using the equations in (21)

check the bound of the particle velocity

if $v_{ij} > v_{\max j}$, then $v_{ij} = v_{\max j}$
if $v_{ij} < v_{\min j}$, then $v_{ij} = v_{\min j}$

and update position $\mathbf{x}_i$ using equations (22)

check the bound of the position

if $x_{ij} > x_{\max j}$, then $x_{ij} = x_{\max j}$, and set $v_{ij} = 0$
if $x_{ij} < x_{\min j}$, then $x_{ij} = x_{\min j}$, and set $v_{ij} = 0$

End

Step 4. To reduce the chance of getting trapped in a local optimum, the random mutation step for the parameters of each particle is conducted according to the following rules.

If $\text{rand}_3 > 0.95$

Then $j = \lceil D \times \text{rand}_4 \rceil$, $x_{ij} = x_{\min j} + (x_{\max j} - x_{\min j}) \times \text{rand}_5$

where $\lceil\ \rceil$ is a roundup function and N is the identified parameter number. When the random number $\text{rand}_3 > 0.8$, x_{ij}, the j-th parameter of the i-th particle, can be updated randomly at each step. rand_3, rand_4, and rand_5 are the random numbers between $[0, 1]$.

Step 5. Evaluate the fitness function of the particle calculated in Step 2.

If $\text{Fitness}(\mathbf{x}_i(n+1)) < \text{Fitness}(\mathbf{p}_i)$, update personal best $\mathbf{p}_i = \mathbf{x}_i(n+1)$

If $\text{Fitness}(\mathbf{x}_i(n+1)) < \text{Fitness}(\mathbf{p}_g)$, update global best $\mathbf{p}_g = \mathbf{x}_i(n+1)$

If Fitness $(\mathbf{p}_g) > 10^{-7}$ and $n \leq \Xi$, $n = n+1$, go to Step 3

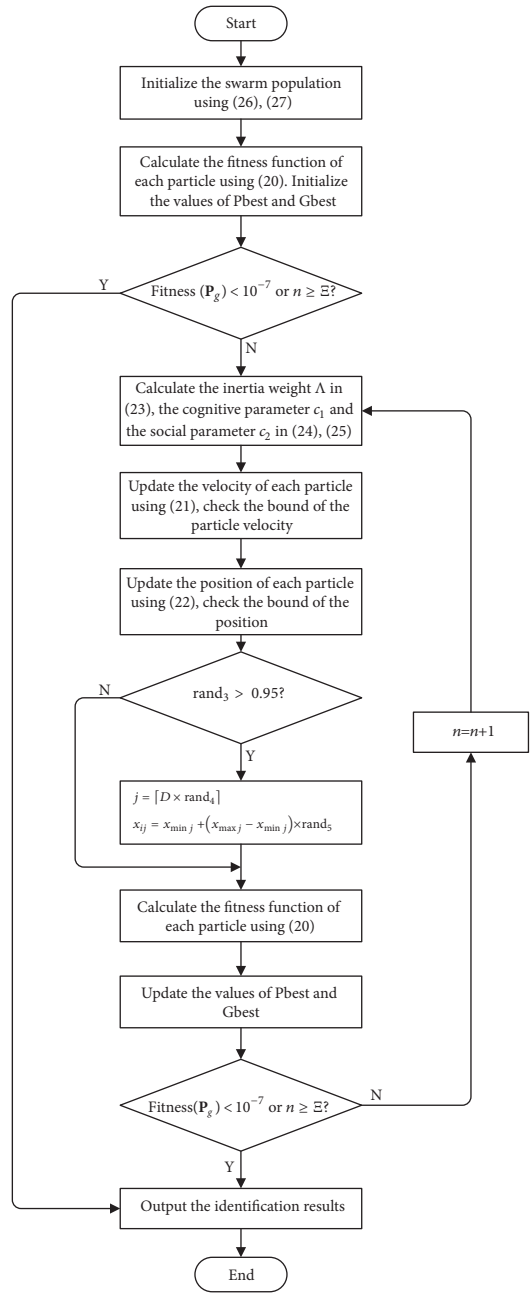

Figure 4: The flowchart of the modified PSO algorithm.

Step 6. If Fitness $(\mathbf{p}_g) < 10^{-7}$ or $n \geq \Xi$, the global solution $\mathbf{p}_g = (p_{g1}, p_{g2}, p_{g3}, p_{g4}, p_{g5})$ is obtained, stop.

Remark 3. Usually, the cognitive parameter c_1 and social parameter c_2 satisfy $c_1 \gg c_2$, and it can improve the capability of searching the global optimal value. Since the cognitive parameter c_1 and social parameter c_2 are related to the number of iterations, the parameters c_1 and c_2 show the flexibility with the change of the number of iterations.

5. Experiment Verification

In this section, the results of applying the proposed modified PSO identification algorithm for the Jiles-Atherton model are given. The results are illustrated by comparing the modeling results with experimental data acquired for the SMA-based compliant actuator platform introduced in Section 2.

For the Jiles-Atherton model defined in Section 5, there are 5 parameters to be identified, so the position vector $\mathbf{x}$ of each particle can be defined as $\mathbf{x} = [\alpha, a, k, M_s, c]$. In addition, to verify the validity of the proposed algorithm, the basic PSO algorithm is also applied for the parameter identification of Jiles-Atherton model in the test.

Using the experimental results for the PWM signal's cycle as 60s with amplitude 5V and duty cycle as 50% given in Figure 3, the search space of basic PSO and modified PSO algorithms for 5 parameters is given in Table 1. The maximum

Table 1: Parameters search space.

Parameters	Min	Max
α	1e-14	1e-2
a	1e-2	1e4
k	1e-2	1e4
M_s	1e5	3e7
c	1e-2	3

Table 2: Parameter identification results.

Parameter	Basic PSO	Modified PSO
α	1.000e-14	1.000e-14
a	7.982261	9.771736
k	58.11999	33.80507
Ms	2.2722e7	2.6155e7
c	1.552548	1.938721
Fitness	3.611e-4	3.296e-4

of search velocity is also set as 15% of the search space for basic PSO and modified PSO (MPSO) algorithms.

In the basic PSO and the modified PSO algorithms, the size of the swarm is selected as 50 and the maximum iteration number as 300. For the basic PSO algorithm, the inertia weight Λ is set as 0.9 and the cognitive parameter c_1 and social parameter c_2 are both selected as 0.5. For the modified PSO algorithm, the initial value and the final value for the inertia weight, cognitive parameter, and social parameter are chosen as $\Lambda_{\max} = 0.9$, $c_{1\text{ini}} = 2.5$, $c_{2\text{ini}} = 0.5$ and $\Lambda_{\min} = 0.4$, $c_{1\text{end}} = 1.3$, $c_{2\text{end}} = 1.7$. Using the parameter initialization method defined in (26), the initial value of the identified parameters can be set randomly in search space, and the particle with the minimum value of fitness function can be chosen as the initial position of $\mathbf{p}_g$.

Following the identification introduced in Section 4, the identification results for 5 parameters in the Jiles-Atherton model are obtained, and the results are given in Table 2. 1210

To illustrate the performance of the proposed algorithm, the fitness functions of basic PSO and modified PSO algorithms are also given in Figure 5. The modified PSO algorithm with the dynamic adjustment for the parameters in the process shows some advantages in the accuracy and the convergence rate compared with the basic PSO algorithm.

In addition, the experiment is conducted by changing the PWM signal's cycle as 60s with amplitude 5V and duty cycle is 50% (Figure 6(a)) to show the accuracy of the proposed identification method. As shown in Figures 6(c)-6(d), the input-output hysteresis loop of the SMA-based compliant actuators between the temperature and the rotation angle is used to verify the modeling performance.

The result of using basic PSO algorithm for Jiles-Atherton model is also provided to show the accuracy of the identification performance. The comparison of hysteresis loops between the experimental data and the Jiles-Atherton model calculated using different identification results are given in

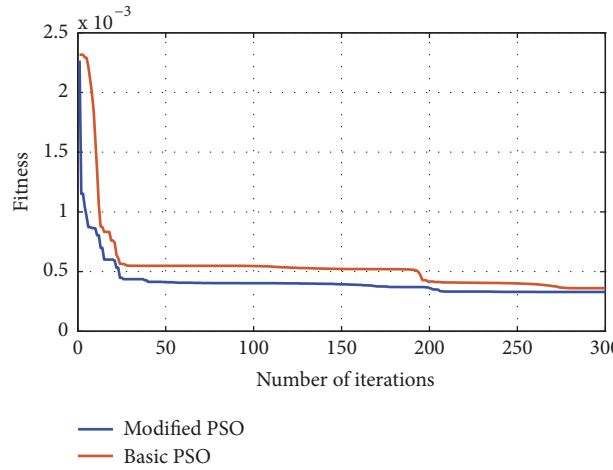

Figure 5: Comparison of fitness function between the basic PSO algorithm and the modified PSO algorithm (red line: basic PSO; blue line: modified PSO).

Figure 7 with the absolute errors in Figure 8. It can be observed that the maximum errors of the radiation angle response are about 30.84% of BPSO case and 22.53 % of MPSO case, respectively. The parameters using MPSO method are more effective than the basic PSO method for the Jiles-Atherton model describing the output characteristics of the SMA-based compliant actuator.

6. Discussion

In this paper, the parameter identification of SMA-based compliant actuating system described by Jiles-Atherton model is addressed. Jiles-Atherton hysteresis model is a differential-equation based hysteresis model, which can describe the saturated hysteresis between the input (voltage or temperature) and output (rotation angle). The accurate identification of these parameters in the Jiles-Atherton model is helpful to estimate the actuator output in the application. For such purpose, a modified PSO identification algorithm is proposed to obtain the Jiles-Atherton hysteresis model parameters. To avoid the local optimum problem in the basic PSO algorithm, the proposed modified PSO algorithm can adjust the location and velocity of each particle by using the random mutation to extend the search space of the solution in the iteration step so that the global optimum can be obtained effectively. The experiment platform is conducted to verify the effectiveness of the proposed identification algorithm, and the comparison results with the basic PSO algorithms are given to illustrate the accuracy of the proposed method.

For this study, some future work to improve the compliant SMA driving performance can be considered. The thermal dynamics between the input current and the temperature is not considered which may cause the system response delay. Besides, the rate-dependent hysteresis properties of the SMA materials also degrade the driving performance when the input signal frequency changes. These issues yield a direction for extension of the hysteresis modeling method with the

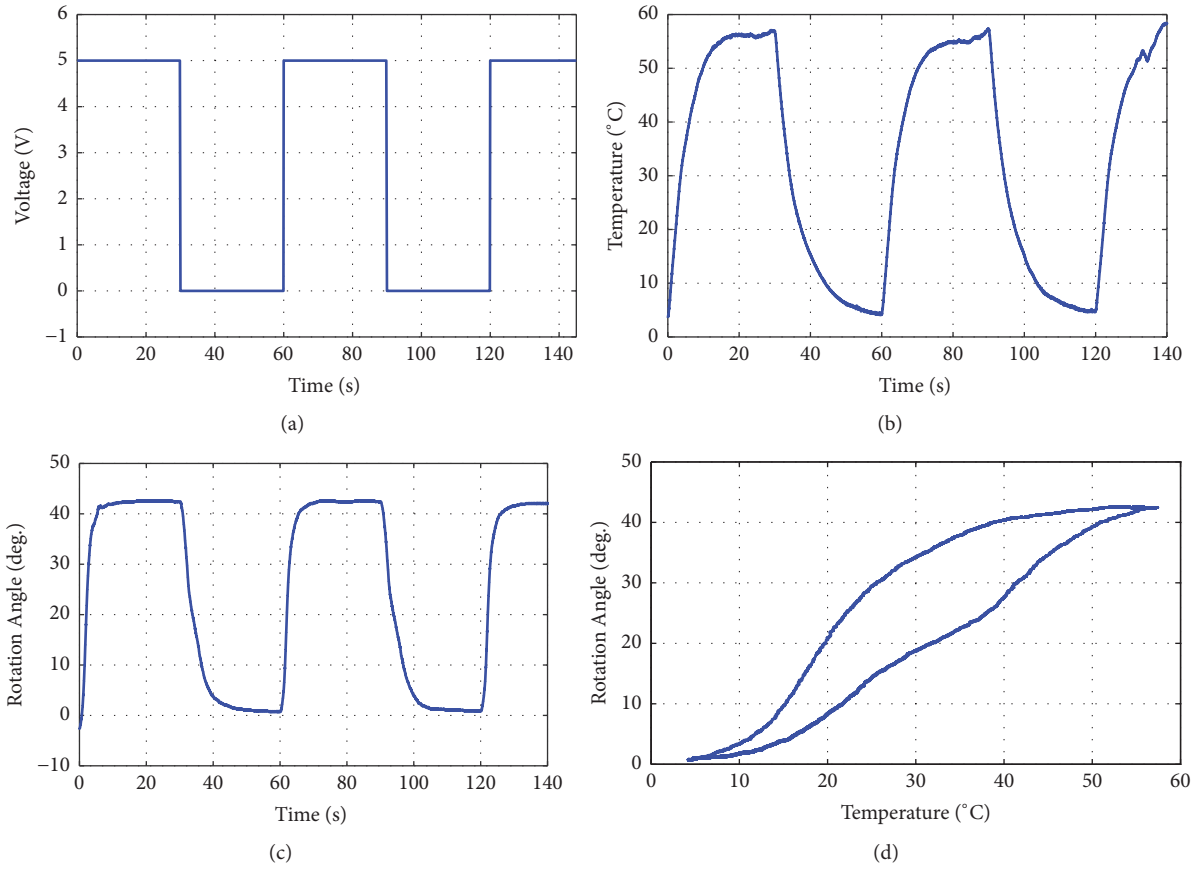

Figure 6: Input-output characteristics of the SMA-based compliant actuators under a fixed duty cycle (50%) 5v PWM signal operation with 60s signal cycle producing the temperature changing between 0°C and 60°C. (a) Input voltage. (b) Input temperature. (c) Output rotation angle. (d) Hysteresis loop.

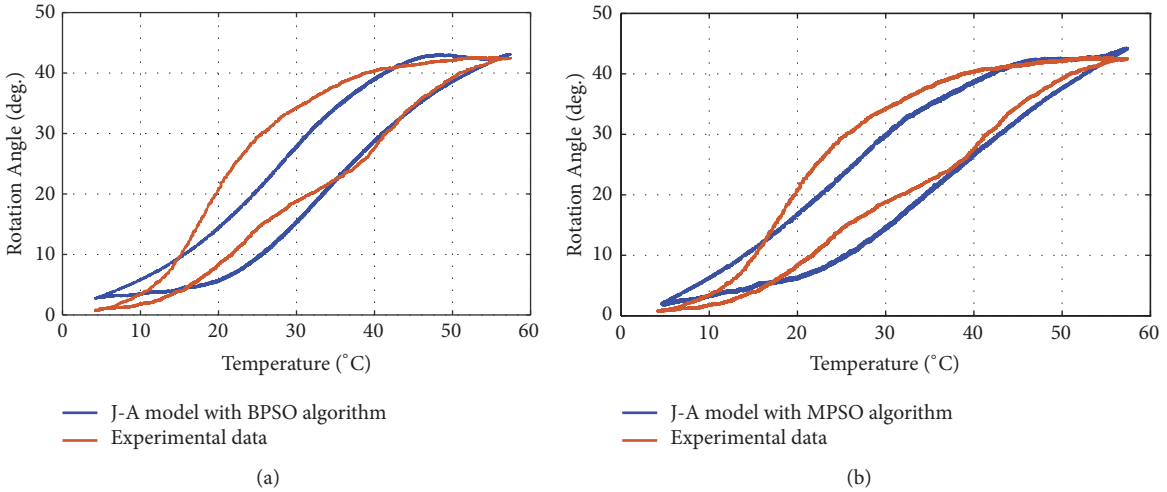

Figure 7: Comparisons of output-input responses between the Jiles-Atherton model with PSO identification algorithm and the measured data (red line: measured data; blue line: J-A model with basic PSO): (a) with basic PSO algorithm and (b) with modified PSO algorithm.

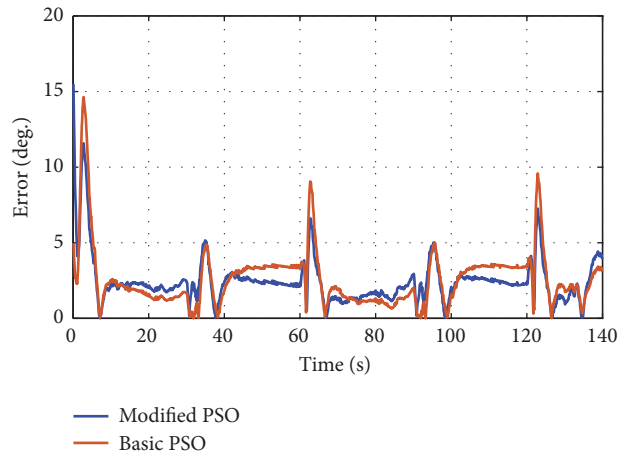

Figure 8: Comparison of modeling error between the Jiles-Atherton model with basic PSO algorithm and J-A model with modified PSO algorithm (red line: J-A model with BPSO; blue line: J-A model with MPSO).

novel identification algorithm. The results of the accurate modeling for SMA-based compliant actuating system can be furthered to conduct the proper controller cancelling the nonlinear effects and improve the driving performance, which would yield the high driving performance of compliant SMA actuators.

Data Availability

The data used to support the findings of this study are available from the corresponding author upon request.

Conflicts of Interest

The authors declare that they have no conflicts of interest.

Acknowledgments

The work was partially supported by the Funds for National Key Research and Development Program of China (2017YFB1302302), Science Foundation of Science and Technology Planning Project of Guangdong Province, China (2017A010102004), the Natural Science Foundation of Guangdong Province (2018A030313331), and the Fundamental Research Funds for the Central Universities (2018MS71).

References

[1] Z. Fan, K. Raun, L. Hein et al., "Application of artificial muscles as actuators in engineering design," in *Advanced Design and Manufacture to Gain a Competitive Edge*, pp. 875–884, Springer, London, UK, 2008.

[2] C.-P. Chou and B. Hannaford, "Measurement and modeling of McKibben pneumatic artificial muscles," *IEEE Transactions on Robotics and Automation*, vol. 12, no. 1, pp. 90–102, 1996.

[3] M. Salerno, K. Zhang, A. Menciassi, and J. S. Dai, "A novel 4-dof origami grasper with an sma-actuation system for minimally invasive surgery," *IEEE Transactions on Robotics*, vol. 32, no. 3, pp. 484–498, 2016.

[4] V. Bundhoo, "Design and evaluation of a shape memory alloy-based tendon driven actuation system for biomimetic artificial fingers," *Computer Scientists*, vol. 2, 2012.

[5] Z. Guo, Y. Pan, L. B. Wee, and H. Yu, "Design and control of a novel compliant differential shape memory alloy actuator," *Sensors and Actuators A: Physical*, vol. 225, pp. 71–80, 2015.

[6] J. Zhong, X. Zhou, and M. Luo, "A New Approach to Modeling and Controlling a Pneumatic Muscle Actuator-Driven Setup Using Back Propagation Neural Networks," *Complexity*, vol. 2018, Article ID 4160504, 9 pages, 2018.

[7] X. Chen and C.-Y. Su, "Adaptive control for ionic polymer-metal composite actuators," *IEEE Transactions on Systems, Man, and Cybernetics: Systems*, vol. 46, no. 10, pp. 1468–1477, 2016.

[8] X. Chen, C.-Y. Su, Z. Li, and F. Yang, "Design of implementable adaptive control for micro/nano positioning system driven by piezoelectric actuator," *IEEE Transactions on Industrial Electronics*, vol. 63, no. 10, pp. 6471–6481, 2016.

[9] C. Yang, J. Luo, Y. Pan, Z. Liu, and C. Su, "Personalized variable gain control with tremor attenuation for robot teleoperation," *IEEE Transactions on Systems, Man, and Cybernetics: Systems*, vol. 48, no. 10, pp. 1–12, 2017.

[10] C. Yang, C. Zeng, C. Fang, W. He, and Z. Li, "A dmps-based framework for robot learning and generalization of humanlike variable impedance skills," *IEEE/ASME Transactions on Mechatronics*, vol. 23, no. 3, pp. 1193–1203, 2018.

[11] M. Moallem and V. A. Tabrizi, "Tracking control of an antagonistic shape memory alloy actuator pair," *IEEE Transactions on Control Systems Technology*, vol. 17, no. 1, pp. 184–190, 2009.

[12] J. Zhang and Y. Yin, "SMA-based bionic integration design of self-sensor-actuator-structure for artificial skeletal muscle," *Sensors and Actuators A: Physical*, vol. 181, pp. 94–102, 2012.

[13] C. Yang, Y. Jiang, W. He, J. Na, Z. Li, and B. Xu, "Adaptive parameter estimation and control design for robot manipulators with finite-time convergence," *IEEE Transactions on Industrial Electronics*, vol. 65, no. 10, pp. 8112–8123, 2018.

[14] G. Song, V. Chaudhry, and C. Batur, "Precision tracking control of shape memory alloy actuators using neural networks and a sliding-mode based robust controller," *Smart Materials and Structures*, vol. 12, no. 2, pp. 223–231, 2003.

[15] X. Chen, Y. Feng, and C.-Y. Su, "Adaptive control for continuous-time systems with actuator and sensor hysteresis," *Automatica*, vol. 64, pp. 196–207, 2016.

[16] J. Yin, X. Chen, S. Zhang, H. Zhang, and B. Shen, "Characterizing interactions in exchange-spring magnets using a mean field Stoner-Wolhfarth model," *Journal of Physics D: Applied Physics*, vol. 34, no. 4, pp. 514–517, 2001.

[17] I. D. Mayergoyz, *Mathematical Models of Hysteresis*, Springer, New York, NY, USA, 1991.

[18] X. Zhang, Z. Li, C.-Y. Su, and Y. Lin, "Robust adaptive output-feedback control for a class of nonlinear systems with hysteresis compensation controller," *International Journal of Adaptive Control and Signal Processing*, vol. 31, no. 11, pp. 1636–1654, 2017.

[19] Y. Feng, Z. Li, S. Rakheja, and H. Jiang, "A modified prandtl-ishlinskii hysteresis modeling method with load-dependent delay for characterizing magnetostrictive actuated systems," *Mechanical Sciences*, vol. 9, no. 1, pp. 177–188, 2018.

[20] R. Xu, X. Zhang, H. Guo, and M. Zhou, "Sliding mode tracking control with perturbation estimation for hysteresis nonlinearity of piezo-actuated stages," *IEEE Access*, vol. 6, pp. 30617–30629, 2018.

[21] D. C. Jiles, J. B. Thoelke, and M. K. Devine, "Numerical determination of hysteresis parameters for the modeling of magnetic properties using the theory of ferromagnetic hysteresis," *IEEE Transactions on Magnetics*, vol. 28, no. 1, pp. 27–35, 1992.

[22] K. Chwastek and J. Szczyglowski, "Estimation methods for the Jiles-Atherton model parameters A review," in *Proceedings of the 2nd Symposium on Applied Electromagnetics, Poland*, pp. 33–40, 2008.

[23] Y. Yang, B. Yang, and M. Niu, "Parameter identification of Jiles–Atherton model for magnetostrictive actuator using hybrid niching coral reefs optimization algorithm," *Sensors and Actuators A: Physical*, vol. 261, pp. 184–195, 2017.

[24] J. Kennedy and R. Eberhart, "Particle swarm optimization," in *Proceedings of the IEEE International Conference on Neural Networks (ICNN '95)*, vol. 4, pp. 1942–1948, Perth, Western Australia, November-December 1995.

[25] F. Marini and B. Walczak, "Particle swarm optimization (PSO). A tutorial," *Chemometrics and Intelligent Laboratory Systems*, vol. 149, pp. 153–165, 2015.

[26] K. E. Parsopoulos and M. N. Vrahatis, "Recent approaches to global optimization problems through particle swarm optimization," *Natural Computing*, vol. 1, no. 2-3, pp. 235–306, 2002.

[27] X. Gao and R. Liu, "Multiscale chebyshev neural network identification and adaptive control for backlash-like hysteresis system," *Complexity*, vol. 2018, Article ID 1872493, 9 pages, 2018.

[28] E. D. M. Hernandez, C. S. Muranaka, and J. R. Cardoso, "Identification of the Jiles-Atherton model parameters using random and deterministic searches," *Physica B: Condensed Matter*, vol. 275, no. 1-3, pp. 212–215, 2000.

[29] Y. Shi and R. Eberhart, "A modified particle swarm optimizer," in *Proceedings of the IEEE International Conference on Evolutionary Computation and IEEE World Congress on Computational Intelligence*, (Cat. No.98TH8360), pp. 69–73, Anchorage, AK, USA, May 1998.